Experimental Mechanics (2014) 54:1687–1696
DOI 10.1007/s11340-014-9911-1

A New Methodology for Uniaxial Tensile Testing of Free-Standing Thin Films at High Strain-Rates

E. Ben-David · T. Tepper-Faran · D. Rittel · D. Shilo

Received: 6 December 2013 / Accepted: 10 June 2014 / Published online: 21 August 2014

Abstract The investigation of strain-rate effects on the mechanical response and characteristics of thin free-standing films is crucial for the design and fabrication of more reliable MEMS devices. It is also of high interest from the scientific and materials engineering views. In this paper we present a novel apparatus and a procedure for tensile testing of thin free-standing films under a wide range of strain rates from quasistatic to high, almost comparable with those obtained in Hopkinson bar tests. To provide this capability, a unique displacement measurement method is applied and a micro device which meets several strict requirements is implemented. We describe recent results of quasistatic experiments performed on pure aluminum free-standing thin films. A high rate experiment which demonstrates the setup capabilities is also presented. The micro-device measured properties are compared with finite element analysis results.

Keywords High strain rate · Thin films · Mechanical properties · Tensile tests · MEMS

Introduction

Thin metallic films are commonly employed in Micro/Nano Electro Mechanical Systems (MEMS/NEMS), e.g. transducers, switches etc. [1] and are frequently subjected to various mechanical constraints, which may result in plasticity, wear, creep, or fatigue [2, 3]. Thus, the design of more reliable and sophisticated thin-film-based-devices relies on the ability to characterize and control the mechanical properties of thin films. A main characteristic of thin films is that the specimen dimensions become comparable to the characteristic length-scales that govern the mechanical behavior. Therefore, specimens at the μm and sub-μm scales often exhibit a mechanical behavior which may be different from that of bulk specimens, referred to as "size effect". Arzt [4] reports that the fabrication of thin films, multilayer and micro-machined components used in microelectronic and micromechanical systems requires materials to be tailored to small component dimensions. In these cases, the physical mechanism that governs the mechanical behavior may begin to "feel" the presence of the surface or an interface; as a result, a dimensional constraint can appear which superimposes on that of the microstructure.

Another important characteristic of thin films is that the mechanical properties of thin films are strongly dependent on the deposition technique, the fabrication process and the substrate. For example, Espinosa et al. [5] reported a significant hardening effect in Au films with thickness below $0.5\,\mu m$ which has not been observed by Emery and Povirk [6] who studied Au films in the same range of thicknesses, and used similar deposition techniques but had different substrates and fabrication process. Thus, at the current stage it is almost impossible to predict the mechanical properties of thin films, unless specimens from the same processing procedure have been tested to some extent.

Over the years, the difficulties in producing and handling μm-scale free standing specimens, have led to the development of several methods for studying the mechanical behavior of thin films which are attached to a substrate, such as nano-indentation [7] and micro-beam bending test [8]. However, the mechanical behavior of such films is significantly influenced by the substrate and often governed by the kinetics of misfit dislocations at the interface as suggested by Spearing [9]. The interface with the substrate restricts dislocation formation and

E. Ben-David (✉) · D. Rittel · D. Shilo
Department of Mechanical Engineering, Technion- Israel Institute of Technology, Haifa 32000, Israel
e-mail: bderan@tx.technion.ac.il

T. Tepper-Faran
Microsystems Department, R&D and Technology Center, MANOR A.D.T Div., Rafael Advanced Defense Systems, Haifa 3102102, Israel

motion, which results in very high strengths at low thicknesses.

There are several methods for studying the mechanical properties of thin films which are released from the substrate, including bulge test [10], contact loading test [11], and the tensile test [6, 12, 13]. Tensile test benefits from two major advantages: First it is almost not influenced by the film substrate. The substrate does influence the growth stresses which are relevant for any kind of test. Moreover, the substrate itself does not have any influence during the measurement of the film response itself. Secondly, the extraction of the mechanical properties of the specimen is much simpler, since stress and strain states are uniform during the test.

Thin films in MEMS devices may be subjected to a wide range of operating velocities and frequencies, depending on their use, environmental conditions and method of actuation. A device can be used as a transducer for long term measurements, which implies quasistatic loads, or alternatively as a switch [14–16] which mostly dictates high rates and dynamic loads. Hence, in order to design devices that may last and perform under various loading regimes, the investigation of the mechanical properties of thin films at various rates is crucial.

Mechanical testing at various strain rates is also a fundamental problem in materials mechanics. The strain rate can affect the yield stress and ductility in cases where these characteristics are governed by thermally activated processes. Moreover, above some critical strain rate there is not enough time for the heat generated by the deformation to leave the specimen and therefore the deformation process changes from fully isothermal to fully adiabatic. The result is a significant increase of the temperature in a local narrow band, which may induce a strain softening response leading to a different mode of failure known as adiabatic shear band [17, 18]. The critical strain rate above which this thermo-mechanical instability process takes place is still unclear. The study of this problem is hampered by limitations of the existing experimental methods, which allow an application of strain rates either below $\sim 1 s^{-1}$ (by means of large-scale tensile instruments) or above $\sim 500 s^{-1}$ (by means of impact techniques). Therefore, there is a range of strain rates spanning roughly two orders of magnitude where it is difficult to obtain reliable mechanical characteristics. Many common engineering applications, including automotive crash and low-velocity impact, lead to strain rates in this range. However, while the above statement applies to bulk material testing, high strain rate testing of free standing thin films is virtually unexplored as of today.

In principle, tensile testing of thin free standing films has the capability to bridge over the above mentioned gap of strain rates and allow testing at a variable rate from the quasistatic regime up to about $1{,}000 s^{-1}$. The strain rate in tensile tests is given by:

$$\dot{\varepsilon} = \frac{v}{L} \tag{1}$$

where v is the crosshead velocity and L is the specimen length. Commercial small-scale actuators can provide adjustable velocity of up to $\sim 0.1 m/s$. Thus, for a specimen length of about $\sim 100\ \mu m$ a strain rate of up to $10^3 s^{-1}$ can be obtained in principle.

Despite the physical capability for obtaining high strain rates, none of the previously developed setups for tensile testing of thin free-standing films has allow reaching such strain rates. In fact, most of the previously developed setups (Emery and Povirk, 2002 [19, 20]; Chasiotis et al., 2007 [21]; Li and Cima, 2004 [22]) are limited to very slow (quasistatic) strain rates. Recently, Jonnalagadda et al. (2009) [23] and Jonnalagadda et al. (2010) [24] investigated the rate dependency of Pt and Au thin films. By using relatively fast microscopy system, they succeeded to achieve strain rates of 10 s^{-1}, which is the physical limit of their system. Their results exhibit some increase of the yield stress and a decrease of ductility at higher strain rates above $0.1 s^{-1}$. Yet, the same mechanical process, thermally activated dislocation glide, was responsible for the plasticity in all strain rate regimes.

The main problems associated with tensile testing of free standing films at high strain rates comes from the short duration of the overall test. The latter can be estimated by $\Delta t = \varepsilon_f / \dot{\varepsilon}$, where ε_f is the strain at failure. Thin metallic films tend to be more brittle than bulk materials and usually exhibit ε_f of about 5 % [5, 6]. Thus, the overall test duration at a strain rate of $1{,}000 s^{-1}$ is expected to be $50 \mu s$. This short duration imposes a severe requirement from the bandwidth and sampling rate, which should be much larger than $1/\Delta t$ for all measuring devices. In particular, the displacement measurement system is required to provide a combination of long sensing range, high accuracy and high bandwidth, which is beyond the capabilities of conventional methods for measuring displacements of micro devices. In order to solve this problem, we reported previously a novel implementation of an optical encoding method for measuring displacements of micro devices that provides good capabilities in all of the above mentioned figures of merit [25]. The optical encoding system combines a commercial reading apparatus with a custom-made metal grating that can be easily produced during MEMS fabrication. In a previous study [25], we demonstrated the ability of this system to measure displacements with a resolution of $25 nm$ and bandwidth above $1 MHz$, under a variety of prescribed velocity profiles.

In this paper, we present a novel apparatus and a method for testing free-standing thin films under choose-able strain rates from the quasistatic regime to about $500 s^{-1}$.

Experimental

Experimental Setup

The experimental setup consists of six main modules, shown in Fig. 1 and described schematically in Fig. 2: (1) A micro device which enables to mount the free-standing film and to protect it from tearing. (2) A piezoelectric linear stage (PI, model P-621.1CD) which applies a controllable displacement on the free-standing film by pulling one side of the micro device (the moving gripper). The stage enables relatively long travel of up to $100\,\mu m$ with nm-scale resolution. (3) A piezoelectric force sensor (Kistler model 9215), which is located on the static gripper and measures the force applied on the micro device. The force sensor measuring range is up to $2\,N$ with a resolution of 50 μN and natural frequency larger than $50\,kHz$. (4) An optical encoder that measures the elongation of the free-standing thin film by measuring the displacement of a micro-grating located on the micro-device. The encoder's measuring range is determined by the grating length and is in the *mm*-scale while its resolution is about $25\,nm$. (5) Mechanical alignment and imaging system that enables to adjust the micro device under the encoder read-head. (6) Designated software and user interface which is used to operate the entire system and to record the measured response. For sampling all of the above transducers a new state of the art scope (not shown in the Figs) has been used (Agilent, model InfiniiVision 4000 X-Series) which allows a sampling rate of up to $1\,GHz$.

Specimen and Micro-Device Design and Fabrication

A top-view picture of the micro-device is sown in Fig. 3. The thin-film sample (a) is attached to a static frame on the right side and to a moveable stage which is suspended on four 'S'-shaped springs (c) on the left side. A metallic encoder grating is fabricated on the surface of the moveable frame to allow measuring its displacement. Circular holes are located on the static frame (e) and the moveable stage (f) to allow mounting the micro device on two pins which serve as grippers.

The springs were designed such that their overall stiffness along the tensile direction is much smaller than the stiffness of the thin film sample. This condition assures that most of the measured force is carried by the sample. The part of the force which is carried by the springs can then be subtracted from the overall measured force in a method which is explained in the

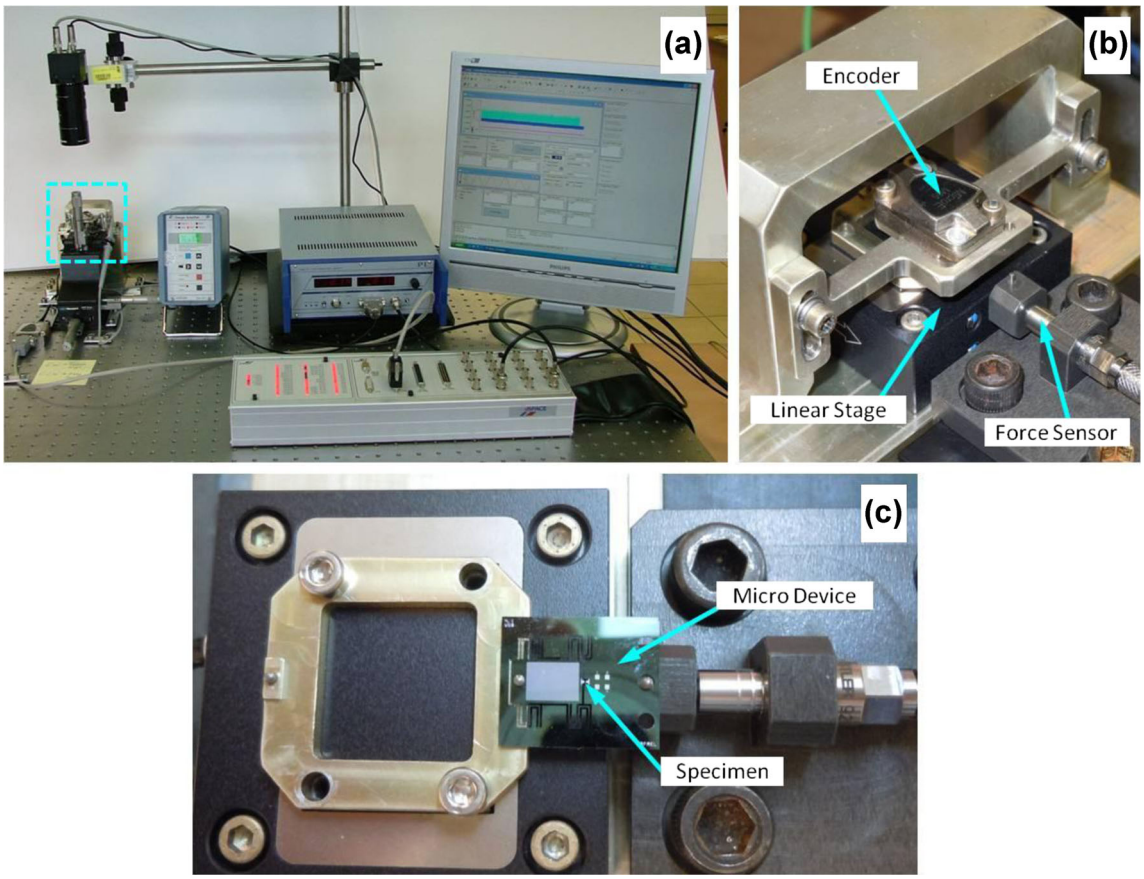

Fig. 1 The experimental setup (**a**) A general view of the system. (**b**) A close-up view of the measuring assembly (the light blue square in view a). (**c**) The micro-device mounted on the measuring assembly between the two grippers

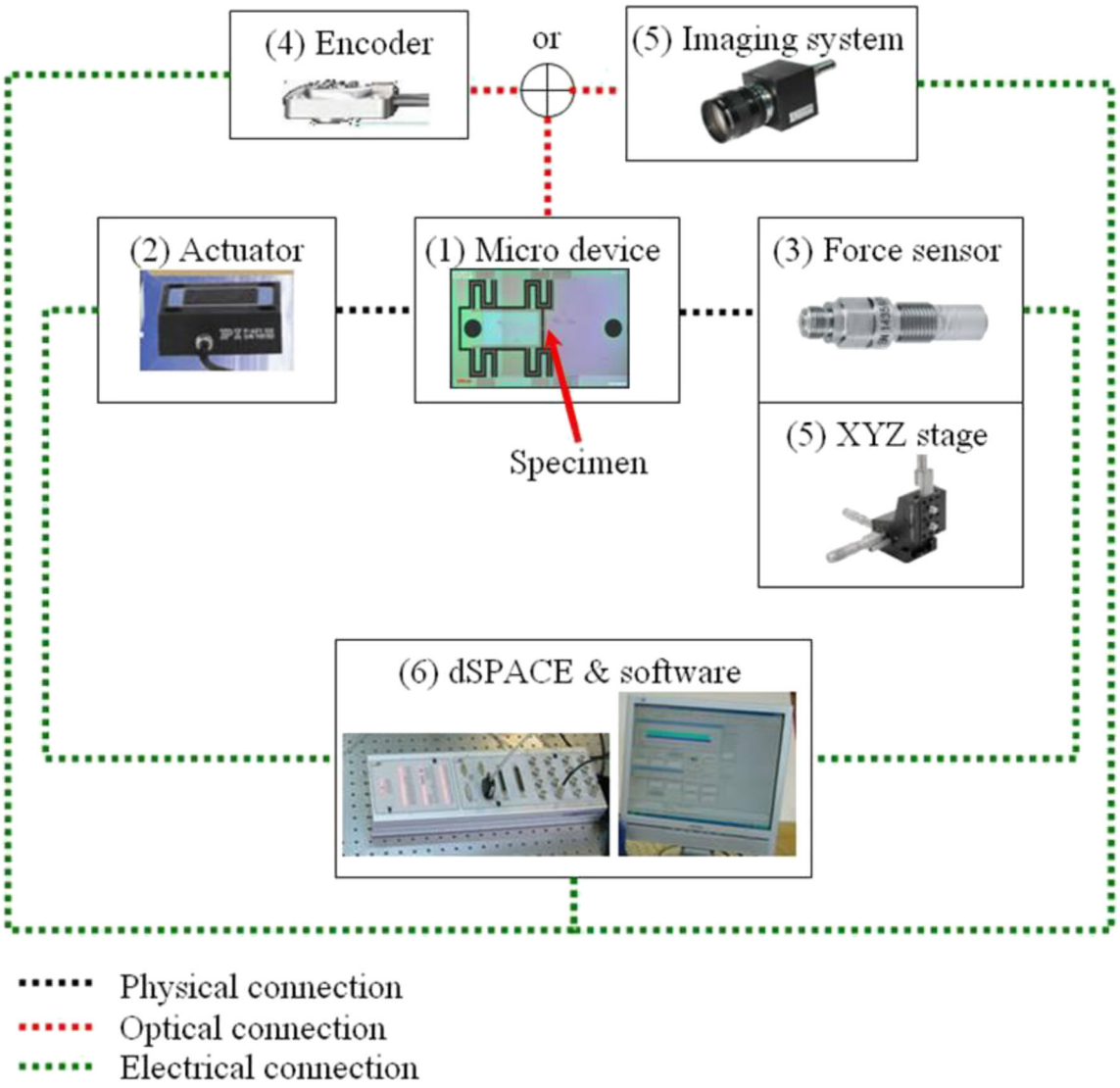

Fig. 2 The experimental setup – block diagram

test procedure section. In order to protect the thin-film sample from tearing, the springs must have large stiffness along directions perpendicular to the tensile axis which are related to bending and torsion of the sample (in these directions the stiffness of the sample is very small). Hence, the springs were designed such that their stiffness along the perpendicular directions is larger than their stiffness along the tensile axis. In addition, the springs' travel was designed to enable specimen's elongation of up to 50 % (i.e. 60 μm) without a failure of the springs. These contradicting requirements, i.e. relatively stiff springs for protection on the one hand, and long travel for specimen's displacement on the other hand, required optimization which was performed using a designated Matlab code.

Finite element (FE) calculations of the overall stiffness of the four 'S' springs provide 3.51 N/mm along the tensile axis, 22.7 N/mm along the direction perpendicular to the tensile axis out of the device plane and 7.75 N/mm along the direction perpendicular to the tensile axis in-plane. For a comparison, the stiffness of a $1\times25\times100\ \mu m^3$ aluminum sample along the tensile axis is expected to be 17.5 N/mm. Both static and modal analyses were used to validate the springs' stiffness. The analyses were performed using shell elements, since thin features are involved. Constrains were assigned in a way that may simulate the real test conditions: six degrees of freedom (DOF) of the static gripper were fixed, where the movable gripper was fixed in only five DOF which enabled elongation in the tensile direction. Silicon elastic constants were taken as $E=130\,GPa$ and $\nu=0.28$ [26].

Static analyses were used for calculating the stiffness along the tensile direction. For this purpose, a displacement was assigned to the movable gripper and the resulted reaction force at the static gripper was calculated. This calculation was repeated with several different displacement values in order to evaluate the springs' stiffness from the received force-

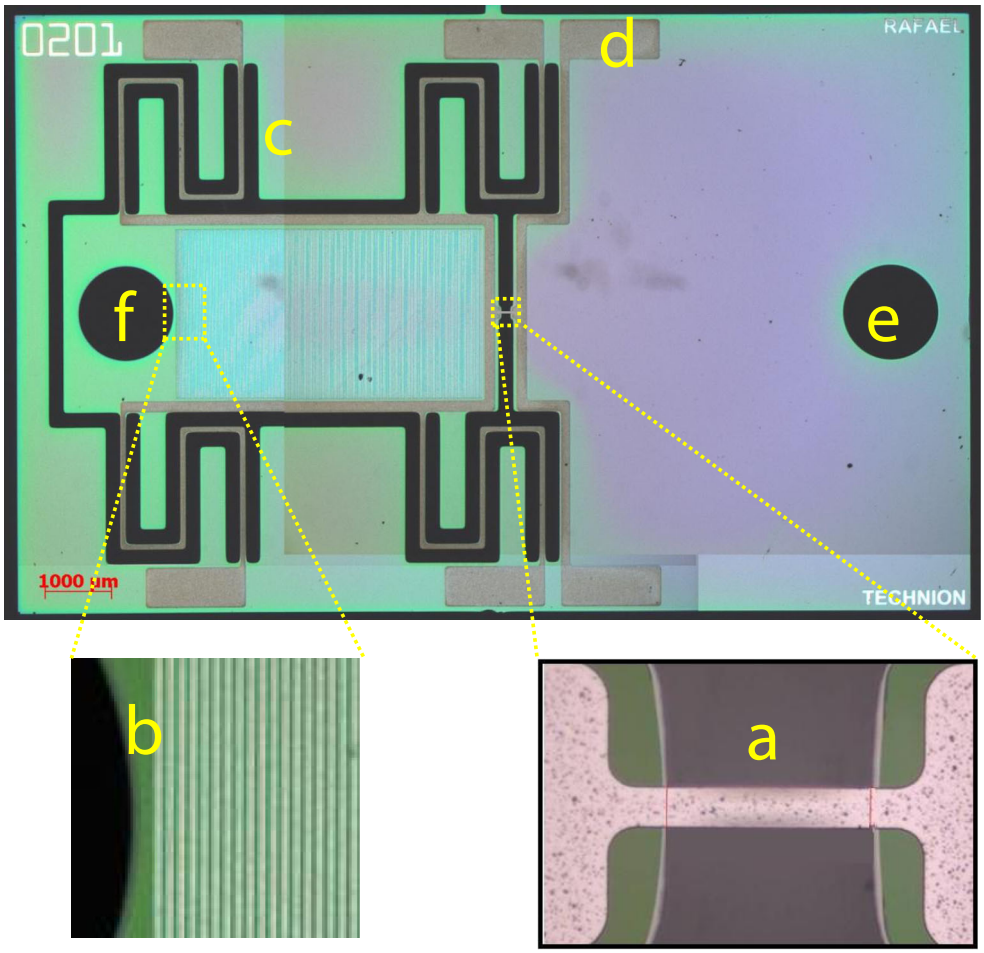

Fig. 3 Micro-tensile specimen (dimensions $13.8\times8.5\,mm^2$) after separation from the wafer: (**a**) Aluminum thin film (specimen). (**b**) Encoder grating for displacement measurements. (**c**) 'S'-shaped springs which allow axial movement. (**d**) Conduction pads for electrodes. (**e**) Static gripper for micro device mounting. (**f**) Moving gripper to apply tension

displacement curve. The modal analyses allows calculating both the resonance frequencies ω_n, which are related to the spring stiffness k via $\omega_n = \sqrt{k/m}$, and the shapes of the vibration modes. The stiffness value along the tensile direction calculated by the modal analysis was in agreement with the value calculated by the static analyses (within a range of± 3 %). The modal analyses provided also the stiffness values along the two directions perpendicular to the tensile direction.

In addition, FE analysis showed that the response time of the 'S'-shaped springs, which is related to the first resonance frequency of an individual spring under its own mass, is about 32 μs, i.e. shorter than the shortest expected test duration. This means that even under the shortest test duration the force vs. displacement response of the springs is still expected to be approximately linear.

The micro-tensile aluminum specimens (shown in Fig. 4) were designed at the Technion in collaboration with Rafael Ltd. and were fabricated at Rafael's MEMS labs. The fabrication procedure is similar to those of references [13, 23, 27] and is described schematically in Fig. 5. The substrate is a Si (001)

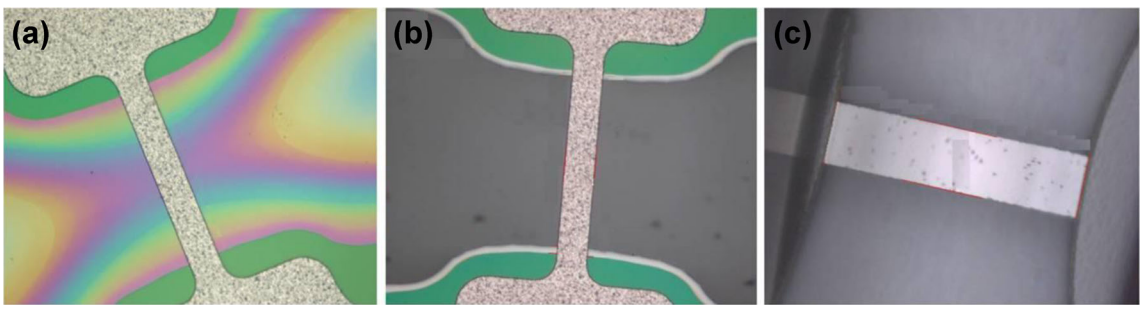

Fig. 4 Zoomed images of an aluminum specimen with a width of $23.8\,\mu m$: (**a**) After DRIE of bulk silicon underneath the aluminum specimen, silicon nitride under the specimen is still present. (**b**) After full release of the specimen by removal of the silicon nitride under layer using RIE (silicon nitride areas on top of the silicon substrate appear green). (**c**) Bottom side of the specimen after release

wafer having a thickness of 250 μm, a diameter of 100 mm , and coating layers of 400 nm super low stress LPCVD silicon nitride (<100 MPa) on both sides (Fig. 5(a)). First, a layer of 1.2 μm aluminum, which defines the dog-bone tensile specimen, is deposited and patterned on side A of the wafer using e-beam evaporation and wet etching (Fig. 5(b)). The sample average grain size was measured by SEM and was found to be 0.18 μm. A second layer of 0.5 μm aluminum, which defines the encoder grating, is then deposited on the same side of the wafer (Fig. 5(c)). The encoder grating was patterned using lift-off deposition, to achieve maximum dimensional accuracy and maximum optical reflectivity. High contrast between the bright aluminum grating and the dark silicon substrate is crucial for proper operation of the encoder read-head. The separate deposition of the dog-bone layer and the encoder grating layer allows one to use the same set of masks and setup to explore the mechanical properties of thin films made of various materials. The alignment of the two layers was better than 0.5 μm and 0.003°. Next, reactive ion etching was used to clear the top silicon nitride layer in areas that are later going to become through holes in the silicon wafer (Fig. 5(d)). This etching is mainly aimed for clearing the gripper holes from possible silicon nitride residues, thus assuring that during the tensile test the pins will be in contact with a bulk Si substrate rather than a residue of thin silicon nitride layer. Following this, the silicon nitride layers and the silicon wafer were patterned on side B and etched using RIE and DRIE in order to define the tensile 'S'-shaped springs and remove the silicon underneath the metal layer (Fig. 5(e)–(g)). The specimens were manually separated from the wafer by cleaving dedicated tabs that attached each specimen to the wafer frame.

About 90 % of the thin film samples were torn during the fabrication and handling process due to two main reasons. First, as will be shown in the quasistatic experiments section, the aluminum thin films are very brittle. As a result, part of them was failed when the micro-device was separated from the wafer or from the gel pack which was used for handling. Second, a non-uniformity of the bulk silicon etching by DRIE (stage f in Fig. 5) resulted in a partial etching of the top silicon nitride layer in part of the wafer regions. This led to cracks in the silicon nitride layer which penetrated into the aluminum film.

All other functional features of the micro-device demonstrated excellent uniformity. All acute features such as 'S'

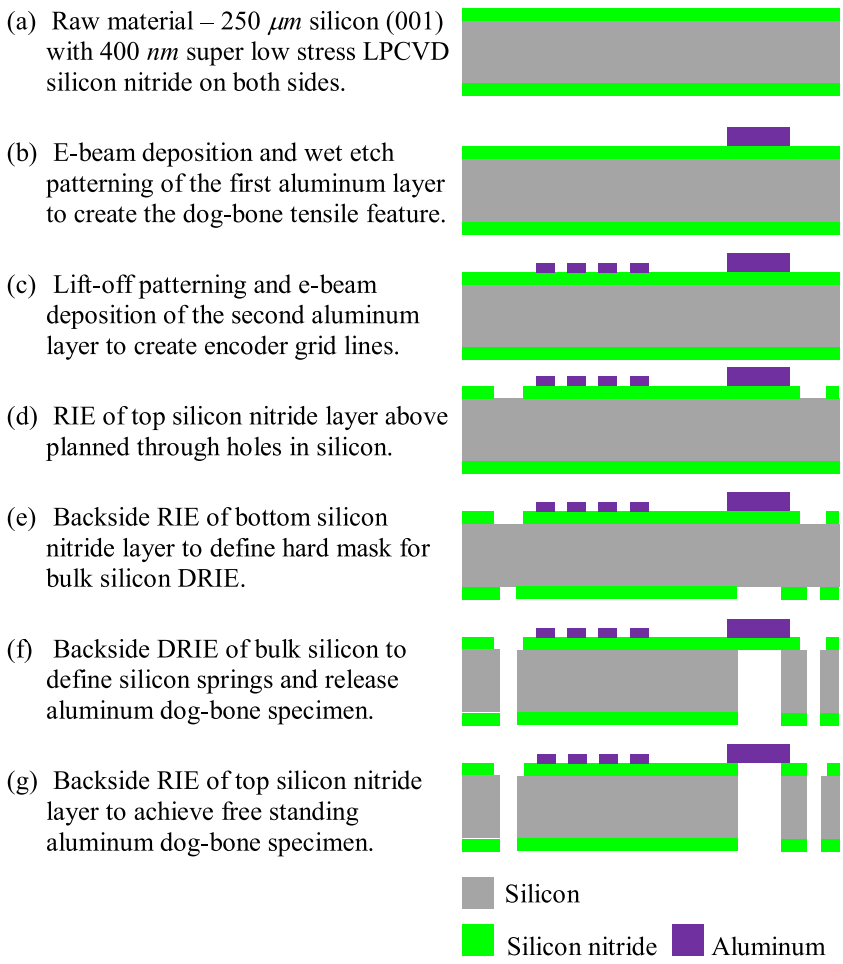

Fig. 5 Fabrication steps for micro-tensile aluminum specimens

shaped springs and gratings stripes where measured based on SEM images for all fabricated micro-devices. The width of aluminum stripes in the encoder grating is of great concern, since a deviation from its prescribed value ($10\,\mu m$) may result in an error in displacements measurements. The grating uniformity was measured and found to be $10\pm0.06\,\mu m$ which is well within the encoder read head requirements.

Test Procedure

The test procedure begins with mounting the micro-device between the two pin grippers as shown in Fig. 1(c). At this stage, the imaging system is placed over the micro-device and misalignment between the micro-device and the linear stage is corrected by the XYZ-stage. The imaging system is then removed and the encoder read-head is placed over the micro-device. The encoder enables relatively large angular misalignment error (up to ±2°). The entire system is then triggered for the beginning of the test. A choose-able displacement signal is fed to the linear stage actuator to generate motion. As the gripper which is attached to the linear stage starts moving, tension is applied to the micro-specimen until it is torn. Then the signal changes sign to unload the springs, followed by a reloading step to measure the response of the springs alone. Thus, two tests are performed in series. In the first test, the response of both the springs and the specimen is measured. In the second test, after the specimen is torn, only the spring's response is measured. The force measured over the springs alone is subtracted from the force measured over the springs and the specimen to extract the specimen's response alone.

Results and Discussion

In this part of the article, we first demonstrate the capabilities of the new experimental setup for applying high strain rates and measuring the mechanical response with a desired accuracy and temporal resolution. Due to a small number of qualified micro devices with an intact thin film sample, we discuss the above mentioned issues based on a high speed test of a micro device without a sample, i.e. a tensile test of the silicon springs alone. This test provides a demonstration of the force and displacement measurements with a suitable resolution and bandwidth. In addition, this test shows that under high speed tests the force vs. displacement response of the silicon springs is still linear with the same stiffness (slope) as in quasistatic tests. Thus, in future high strain rate tests with samples, the force carried by the springs can be calculated based on their elongation and subtracted from the overall force with an aim of extracting the force carried by the sample.

In the quasistatic experiments section, one of the quasistatic tests, which have been taken with a thin free-standing aluminum film, is presented. We demonstrate the overall test procedure and analysis and discuss the quality of the obtained results.

High Rate Experiments

Figure 6 shows a typical high speed test which has been taken with silicon springs only. In order to obtain a high velocity at which the springs are pulled, a step command is inserted to the piezoelectric actuator (green curve in Fig. 6(a)). Due to the inertia of the actuator stage, the actual displacement of the actuator (red curve in Fig. 6(a)) is not instantaneous and it takes about 20 μm for the actuator to obtain the maximal velocity. Therefore, a gap of about 23 μm between the gripper pin and the edge of the circular hole is left intentionally, such that when the pin is reached to a contact with the edge of the moveable silicon stage it already has the maximal velocity provided by the actuator. The initial increase of the force signal is marked by point 'a' in Fig. 6(b) and it correlates with the first increase of the encoder signal (cyan curve in Fig. 6(a)), which is related to the motion of the moveable silicon stage and the elongation of the springs. Between points 'a' and 'b', the encoder motion is very slow and the slope of force rises gradually. At this stage, the pin gripper slides along the edge of the circular hole such that its motion is not directly transferred to a motion of the moveable stage. After point 'b', both the encoder motion and the force increase with an almost constant slope, which is related to the linear response of the spring. At this stage, the tensile test is actually performed. In this experiment, after point 'b' the encoder velocity is $21\,mm/s$. For designed specimen length of $60\,\mu m$, this velocity can provide a strain rate of $350 s^{-1}$. Higher strain rates can be obtained using a shorter specimen or by replacing the current piezoelectric actuator with a faster one.

In Fig. 7 the force vs. elongation of the springs is presented. This data is taken from the rectangular frames marked on Fig. 6. As is observed the force vs. elongation response is almost linear with a minor waviness due to vibrations in the springs. Such a behavior is predicted based on the FE calculation of the resonant frequency of the springs (see discussion in the Specimen and micro-device design and fabrication section). Based on Fig. 7, the overall stiffness of the 'S'-shaped springs is found to be $3.13\pm0.1\,N/mm$. This value deviates by less than 2 % from quasistatic measurements of the spring's stiffness (see quasistatic experiments section). This value is found by calculating the slope of the curve in Fig. 7, i.e. by $\Delta F/\Delta u$ where ΔF is the force change and Δu is the displacement change. Same calculation is performed similarly in the quasistatic experiments as well. Note that the spring's stiffness is smaller by about 11 % from the value which was calculated in the static FE analysis, but this difference can be attributed to MEMS fabrication issues such as fabrication tolerances and under-cuts etching angles.

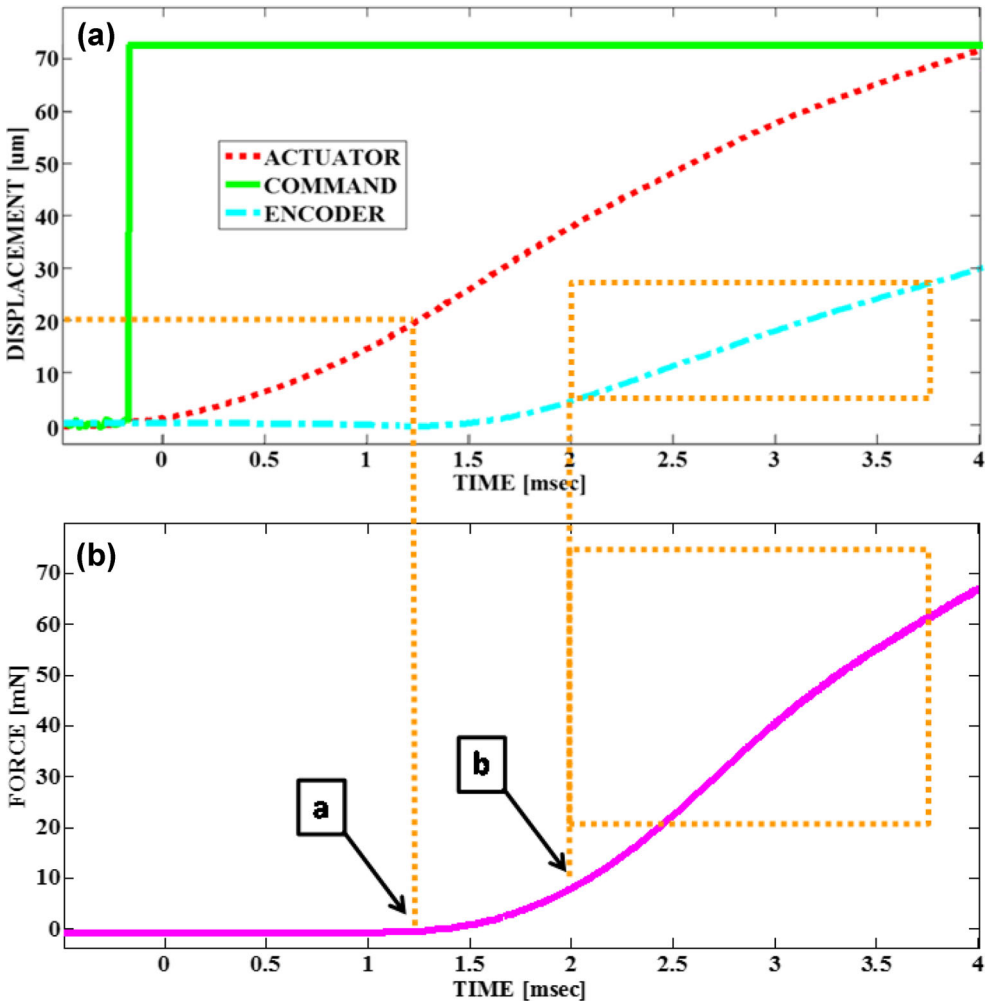

Fig. 6 High speed mechanical tests of the 'S'-shaped silicon springs only. (**a**) Displacements vs. time are shown, where the command which was given to the piezoelectric actuator is shown in green curve, the piezoelectric actuator response is shown in broken red curve and the encoder displacement measurement is shown in dash-doted cyan curve. (**b**) Force measured over the 'S'-shaped springs, is shown in magenta curve. Arrow (**a**) indicates the initial increase of the force signal and it correlates with the initial increase of the encoder signal, which is related to the motion of the moveable silicon stage and the elongation of the springs. Arrow (**b**) indicates the point where both the encoder motion and the force increase with an almost constant slope, which is related to the linear response of the spring

Quasistatic Experiments

The described setup was used to conduct several tests with aluminum specimens. In this section we report a recent result from quasistatic tests performed using the described setup and procedure.

An example for a micro tensile test is presented in Fig. 8 and Fig. 9. The specimen was 105 μ*m* long,

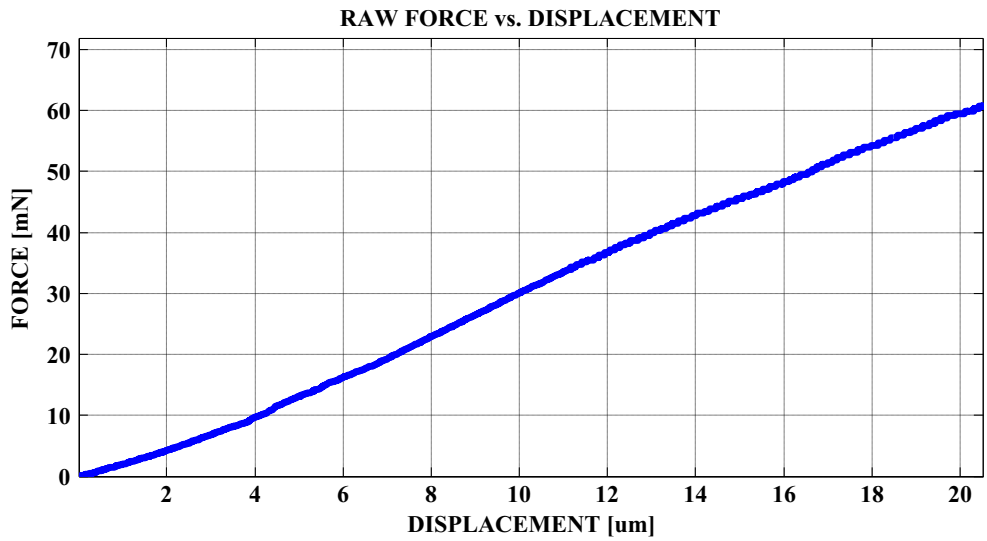

Fig. 7 'S'-shaped silicon springs only response, force vs. displacement. A linear trend is well demonstrated here for high rate test, but also for quasistatic tests as well

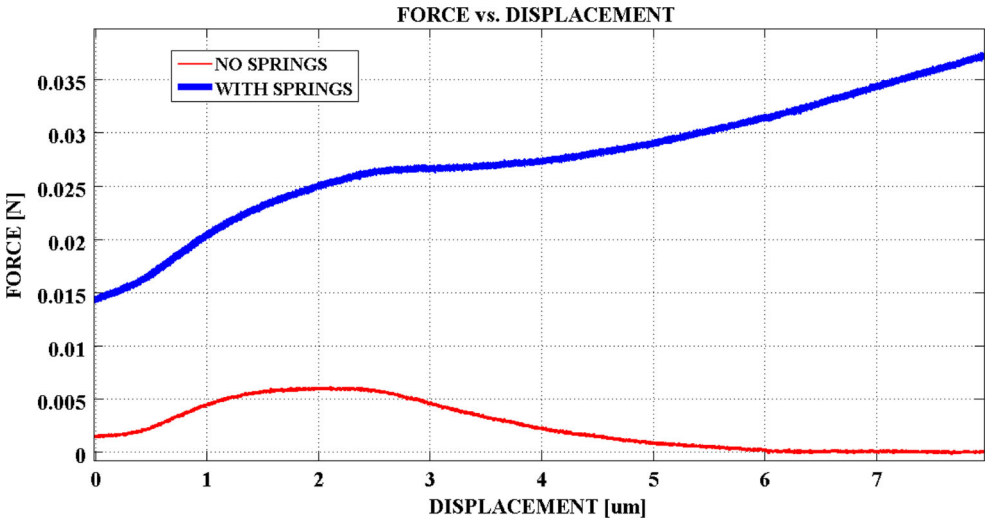

Fig. 8 Force vs. displacement with (blue thick curve) and without 'S'-shaped spring's effect (red thin curve). The 'S'-shaped springs influence has been subtracted to attain the specimen's response alone

23 μm wide and 1.21 μm thick aluminum free-standing film. At this test the actuator velocity was 0.16 $\mu m/s$ and the calculated strain rate based on equation (1) was 1.5e-3s^{-1}. The spring's stiffness, which was calculated based on the force vs. displacement curve in the displacement range of 7–20 μm (beyond the range presented in Fig. 8), i.e. after the sample has been ruptured is 3.06±0.1N/mm. This value is about 2 % smaller than the spring's stiffness of the micro device which has been tested under high speeds (see Fig. 7). In Fig. 8 the force vs. displacement is presented before (blue thick curve) and after (red thin curve) subtracting the force which is carried by the 'S'-shaped springs. The overall force (blue thick curve) doesn't start from zero. This is due to the fact that the springs have been elongated before the sample started to be elongated. This means that the sample has been buckled before the test.

In Fig. 9 the stress vs. strain curve is presented. The yield stress is about 183MPa. The UTS stress is about 212MPa. The elastic strain is about 1.2 % while the plastic stain is about 5 %. The yield and UTS stresses measured in this test are similar to values which have been obtained in three other tests and are also similar to values reported in the literature [28]. The slope of the stress-strain curve is about 16GPa. A similar value, in the range of 16–21GPa, repeated in three other tests. These values are considered to be very low for aluminum films in comparison to the reported Young's modulus of 70.1GPa for pure *bulk* aluminum [29]. This difference is probably a result of the compliance of the mechanical part that connects the static pin gripper with the force sensor. An accurate measurement of the Young's modulus of thin free standing films is a major problem, which appeared in previous studies as well. Several investigators reported similarly low values of Young's Modulus for aluminum thin films in similar kind of tests [29–31]. One can state that our results are well within the reported range.

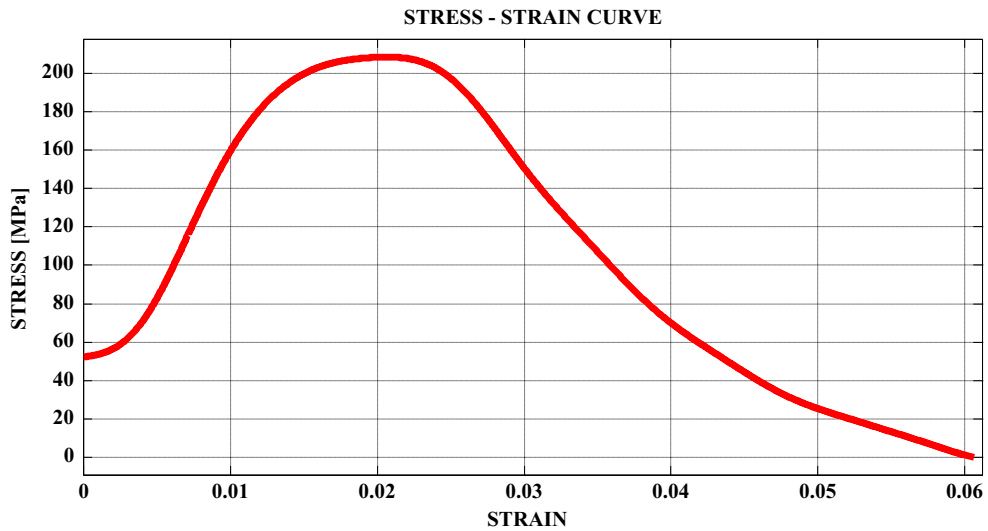

Fig. 9 Stress vs. strain curve of the specimen during the quasistatic test

Summary

In this work we presented and demonstrated a novel experimental setup and methodology for tensile testing of free-standing thin films from quasistatic to high strain rates regimes. We described the experimental setup and the designated micro-device which was designed to allow the fabrication, handling and measurements of the tested thin film. Recent quasistatic results have been presented as well as setup capabilities at the high strain rate regime. Micro-device measured properties have been compared to calculated ones. It is believed that the experimental approach presented in this work will significantly extend the characterization possibilities of free-standing films in a straightforward manner, unraveling in the future their high rate response, the latter being compared with that of the bulk base material.

References

1. Polcawich RG, Pulskamp JS, Judy D, Ranade P, Trolier-McKinstry S, Dubey M (2007) Surface micromachined microelectromechanical ohmic series switch using thin film piezoelectric actuators. IEEE Trans Microwave Theor Techn 55:2642–2654
2. Senturia SD (2001) Microsystem design. Kluwer Academic Publishers, Boston
3. Maluf N (2000) An Introduction to Microelectromechanical Engineering. Artech House, Boston
4. Arzt E (1998) Size effects in materials due to microstructural and dimensional constrains: a comparative review. Acta Mater 46:5611–5626
5. Espinosa HD, Prorok BC, Peng B (2004) Plasticity size effects in free-standing submicron polycrystalline FCC films subjected to pure tension. J Mech Phys Solids 52:667–689
6. Emery RD, Povirk GL (2003) Tensile behavior of free-standing gold films. Part I. Coarse-grained films. Acta Mater 51:2067–2078
7. Srikar VT, Spearing SM (2003) A critical review of microscale mechanical testing methods used in the design of microelectromechanical systems. Exp Mech 43:238–247
8. Kraft O, Volkert CA (2001) Mechanical testing of thin films and small structures. Adv Eng Mater 3:99–110
9. Spearing SM (2000) Materials Issues in Microelectromechanical Systems (MEMS). Acta Mater 48:179–196
10. Kalkman AJ, Verbruggen AH, Janssen GCAM (2001) Young's modulus measurements and grain boundary sliding in free-standing thin metal films. Appl Phy Lett 78:2673–2675
11. Zhang R, Shilo D, Ravichandran G, Bhattacharya K (2006) Mechanical characterization of released thin films by contact loading. J Appl Mech 73:730–736
12. Lee HJ, Cornella G, Bravman JC (2000) Stress relaxation of free-standing aluminum beams for microelectromechanical systems applications. Appl Phy Lett 76:3415–3417
13. Haque MA, Saif MTA (2002) In-situ tensile testing of nano-scale specimens in SEM and TEM. Exp Mech 42:123–128
14. Shen Q, Barker NS (2003) IEEE Radio and Wireless Conference, Boston, MA 313.
15. Zakar E, Polcawich R, Dubey M, Pulskamp J, Piekarski B, Conrad J, Piekarz R (2000) Stress analysis of SiO2/Ta/Pt/PZT/Pt stack for MEMS application. Proceedings of the 12th IEEE International Symposium on Applications of Ferroelectrics, pp. 757–759
16. Peroulis D, Katehi LPB (2003) Electrostatically-tunable analog RF MEMS varactors with measured capacitance range of 300 %. IEEE MTT-S Int. Microw Symp Dig 3:1793–1796
17. Zener C, Hollomon JH (1944) Effect of strain rate upon plastic flow of steel. J Appl Phys 15:22–32
18. Rittel D, Osovski S (2010) Dynamic failure by adiabatic shear banding. Int J Fract 162(1–2):177–185
19. Emery RD, Povirk GL (2002) Tensile behavior of free-standing gold films, part I. coarse-grained films. Acta Mater 51:2067–2078
20. Emery RD, Povirk GL (2002) Tensile behavior of free-standing gold films, part II. fine-grained films. Acta Mater 51:2079–2087
21. Chasiotis I, Bateson C, Timpano K, McCarty A, Barker NS, Stanec J (2007) Strain rate effects on the mechanical behavior of nanocrystalline Au films. Thin Solid Films 515:3183–3189
22. Li Y, Cima MJ (2004) Bulge Test on Free Standing Gold Thin Films Mat. Rec. Soc. Symp. Proc., 795
23. Jonnalagadda KN, Chasiotis I, Yagnamurthy S, Lambros J, Pulskamp J, Polcawich R, Dubey M (2009) Experimental investigation of strain rate dependence of nanocrystalline Pt films. Exp Mech 50:25–35
24. Jonnalagadda K, Karanjgaokar N, Chasiotis I, Chee J, Peroulis D (2010) Strain rate sensitivity of nanocrystalline Au films at room temperature. Acta Mater 58:4674–4684
25. Ben-David E, Kanner O, Shilo D (2009) A new method for measuring displacements of micro devices by an optical encoding system. Exp Mech 49:823–827
26. Hopcroft MA, Nix WD, Kenny TW (2010) What is the young's modulus of silicon? J Microelectromech Syst 19(2):229–238
27. Espinosa HD, Prorok BC, Fischer M (2003) A methodology for determining mechanical properties of freestanding thin films and MEMS materials. J Mech Phys Solids 51:47–67
28. Read DT, Cheng YW, Keller RR, McColskey JD (2001) Tensile properties of free-standing aluminum thin films. Scripta Mterialia 45:583–589
29. Smithells Metals Reference Book (1998). Paperback edition (7th ed.) Oxford: Butterworth-Heinemann
30. Hoffman RW (1989) Nanomechanics of thin films: Emphasis: Tensile properties. Mater Res Soc Symp Proc 130:295–306
31. Stienwall JE (1992) Microfabrication and Mechanical Properties of free standing thin films, PhD Thesis Cornell University, Ithaca, New-York